Langmuir

ARTICLE

pubs.acs.org/Langmuir

Nanoparticle-Enhanced Sensitivity of a Nanogap-Interdigitated Electrode Array Impedimetric Biosensor

Kanwar V. Singh,*[,†] Dheeraj K. Bhura,[†] Gopichand Nandamuri,[†] Allison M. Whited,[†] David Evans,[‡] Jeff King,[§] and Raj Solanki[†]

[†]Department of Physics, Portland State University, 1719 SW 10th Avenue, SB2 Room 134, Portland, Oregon 97201, United States

[‡]Sharp Laboratories, Camas, Washington 98607, United States

[§]Virogenomics, Inc., Tigard, Oregon 97223, United States

Supporting Information

ABSTRACT: Interdigitated electrode (IDE) arrays with nanometer-scale gaps have been utilized to enhance the sensitivity of affinity-based detection. The geometry of nanogap IDEs was first optimized on the basis of simulations of the electric field and current density. It was determined that the gap (G) between the electrodes was the most important geometric parameter in determining the distribution and strength of the electric field and the current density compared to the width (W) and height (H) of the IDEs. Several devices were materialized and analyzed for their sensitivity to the electrochemical environment using faradic electrochemical impedance spectroscopy (EIS) as the detection technique. Nanogap optimized IDEs were then employed as biosensors for the label-free, affinity-based detection of antitissue transglutaminase antibodies (αtTG-Abs), a biomarker for the detection of autoimmune disorder celiac sprue, triggered by ingesting gluten. The label-free biosensor assay was found to be less sensitive compared to on-chip ELISA. Gold nanoparticles (GNPs) were then employed to improve the sensitivity of the nanogap IDE-based biosensor. With GNPs, the transducer sensitivity increased by 350% over that of label-free detection. The suitability of nanogap IDEs as biosensor transducers for EIS in label-free and GNP-labeled formats was established. The immunobiosensor assay detection sensitivity with the GNPs was found comparable to ELISA.

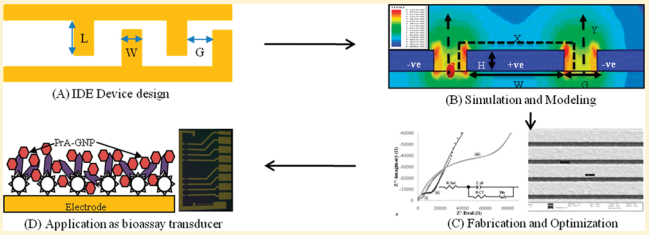

I. INTRODUCTION

The current research in biosensors has focused on the integration of biomolecular probes, signal-enhancing labels, transducers, and their detection apparatus in compact devices. Biosensors based on immunoassays (IAs) have become routine analytical tools in pharmaceutical, toxicological, and environmental analysis as well as in clinical diagnostics because of high sensitivity, high selectivity, rapid detection, and the possible analysis of difficult matrices without extensive pretreatment.[1,2] The introduction of enzyme-labeled reagents in the 1970s revolutionized the field by making IAs reliable, accurate, easier, and safer compared to hazard-prone radioisotope-labeled reagents.[3−6] Enzymatic labels were followed by several other signal-generating methods, most notably fluorophores, chemiluminophores, phosphores, and lately nanoparticles (NPs) that have generated considerable interest as suitable labels for monitoring biomolecular interactions.[7,8] Below we report our results of employing colloidal gold nanoparticles (GNPs) that were used to enhance the sensitivity of an impedimetric immunobiosensor for the detection of specific antibodies in serum samples using immunoaffinity binding interactions. Antibodies (Abs) are produced by the mammalian immune system when non-native molecules (>1kD) called antigens (Ags) are perceived threats. In celiac sprue disease, the gliadin (wheat) peptide gets cross-linked to a lysine residue of tissue transglutaminase (tTG) in a self-catalyzed reaction. The covalent linkage renders tTG as a non-native molecule and triggers the production of αtTG-Abs by the immune system. These anti-tTG Abs in serum are established biomarkers for the specific detection of celiac sprue.[9] The work reported below uses a nanogap-interdigitated electrode array (IDEA) biosensor-based platform to detect antibody−antigen binding events. We have demonstrated the capability of our sensor platform by detecting specific Abs in serum captured with Ag immobilized on a sensor surface and using GNPs for enhanced sensitivity.

Nanoparticles offer several advantages that have attracted widespread interest in their use as labels, including simple chemical processes for biofunctionalization, good biocompatibility, and size comparable to that of most biomolecules.[10,11] Nanoparticles have been prepared from different materials that range from metals (Au, Ag) to semiconductors (CdSe, PbS) to dielectric (TiO_2, SiO_2) materials.[12−15] Colloidal Au NPs have been extensively employed as labels and used to develop a range of immunochemical methods based on visual detection,[15]

Received: July 5, 2011
Revised: September 14, 2011
Published: September 23, 2011

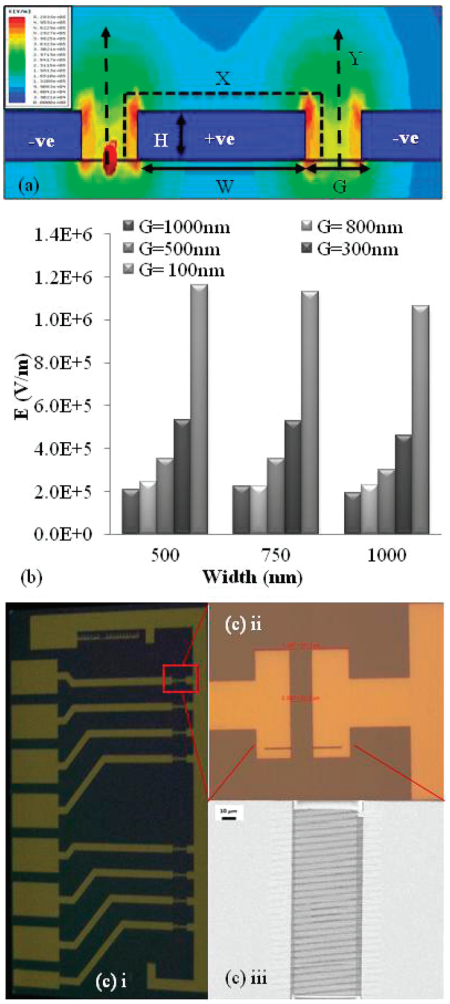

Figure 1. (a) Nanogap IDE design, simulation, and fabricated chip showing the output of the device simulation from the Ansoft Maxwell software for the electric field distribution around the electrodes. The values of the electric field and current density analyzed were determined along the lines marked *X* (50 nm from the electrode surface) and *Y* in the middle of the gap with the following parameters: width (W = 1500 nm), height (H = 200 nm), and gap (G = 500 nm). (b) Bar graph showing the change in the electric field (E) for different width (W) and gap (G) combinations. Please see the Device Simulations section for details. (c-i) Relative placement of IDEs on the IDEA chip. (c-ii) Photomicrograph of blank pads used to make nanogap IDEs using e-beam lithography. (c-iii) SEM section of the same electrode after making nanogap IDEs.

spectrophotometry,[16] electron microscopy,[17] dynamic light scattering,[18] and electrochemical analysis.[19]

Electrochemical detection offers several advantages over conventional optical detection, such as instrument portability, higher performance with lower background, less expensive components, and possible measurements on turbid samples. Electrochemical transducers have often been used to detect biomolecular interactions because of their small dimensions, low cost, and compatibility with micromanufacturing technology.[20,21] However, one major obstacle in implementing electrochemistry for the detection of biomolecular reactions lies in its lower sensitivity as compared to that of optical systems.[20] One of the approaches proposed to enhance the sensitivity is by increasing the number of biomolecular events at the transducer surface by making 3D macroporous gold layers or using nanoporous alumina.[22,23] However, these approaches increase the manufacturing complexity, thereby increasing the production and implementation costs. Another approach includes making electrochemical transducers more sensitive by designing better electrode systems. Most of these approaches aim to bring the sensing elements spatially closer to the biomolecules, which are typically 20−200 nm from the electrode surface.[24,25] Sensor miniaturization based on microelectronic device fabrication technologies has received considerable attention toward the development of such highly sensitive, cost-effective, rapid, reliable, and multiplexed biosensor chips.

The platform for our GNP-based biosensor consisted of nanogap IDEs as the sensing units that are easy to integrate in large-scale arrays. A nanogap-IDE transducer was chosen mainly for two reasons. First, an IDE structure having an interelectrode spacing in the nanometer regime makes it possible to reach high nonstationary as well as stationary electric field strengths with a low applied voltage level that is suitable for biomolecular interactions. Hence, electrode reactions will be lower, and at the same time a high signal-to-noise ratio is obtained.[24] Second, the electric field does not extend far from the electrodes, hence it probes mostly the molecules immobilized on their surfaces, which makes this approach more sensitive.[25]

The geometry of the IDE arrays used for this study was based on simulations that were performed to optimize the main parameters, namely, the width (W), gap (G), and height (H) of the electrodes (Figure 1a), and the length (L) was held constant and was much larger than W, G, or H. These parameters have a significant effect on the electrical characteristics of IDEs.[26,27] Electrochemical impedance spectroscopy (EIS) was used to compare the sensitivity of IDEs with gaps ranging from 100 to 500 nm. A 500 nm gap IDE array was employed to detect antitransglutaminase antibodies (αTGAbs), which are established serum biomarkers for celiac sprue disease. Pr-A-gold nanoparticles (Pr-A-GNPs) were then used to enhance the sensor signal. Our results demonstrate that the biosensor sensitivity was enhanced significantly compared to the label-free detection of αTGAbs. The immunosensor detection assay is also compared with an on-chip ELISA assay for the detection of αTGAbs.

II. MATERIALS AND METHODS

Device Modeling and Simulation. Ansoft Maxwell software was used to model the current density and electric field surrounding the IDEs. It uses finite element method analysis to solve the electromagnetic parameters. The built-in 2D solver option was used for this simulation, where the length of the electrode digits for all IDEs was kept constant and was much larger than the width, gap, and height of the electrodes. The electric field and current density were solved by imposing the following parameters: 1% error allowed, 100% refinement per pass with a maximum of 10 passes, and 1 minimum converged pass. The background medium was PBS, which has a relative permittivity of 80 and a bulk conductivity of 0.13 S/m. The substrate was a 650-μm-thick silicon wafer that was coated with a 1-μm-thick layer of silicon dioxide.

Reagents. Phosphate-buffered saline (PBS) and PBS containing 0.05% tween-20 as a detergent (PBST) were used as the buffer. Potassium ferri/ferrocyanide was used as a redox probe couple at an equimolar concentration of 2.5 mM in PBS for faradic EIS measurements. Tissue transglutaminase (tTG) was purchased from USBio

(Swampscott, MA, U.S.). Goat anti-tTG antiserum (T7066), rabbit anti-goat-IgG HRP conjugate (A5420) secondary antibody, protein-A (P6031), and all other chemicals were purchased from Sigma-Aldrich Chemical Co. (St. Louis, MO, U.S.).The interdigitated electrode array chips were manufactured at SHARP Laboratories of America (Camas, WA, U.S.).

Device Fabrication. A combination of UV photolithography (UVPL) and electron-beam lithography (EBL) was used to fabricate functional nanogap-interdigitated electrode arrays that can be used for the sensitive detection of biomolecular activity. The IDEs were made of gold because of its inertness, available functionalization chemistry, and relative ease of fabrication of chips using existing silicon microelectronic device processing technology. The sensor chip design was based on the secure digital (SD) card format with large contact pads and interconnects as well as the nanogap IDEs that were fabricated in two steps. First, the relatively large contact pads and interconnects were fabricated using standard silicon UV photolithography with ECR-enhanced reactive ion etching (RIE). EBL was then performed to produce nanoscale IDEs on substrates with the previously UVPL-patterned interconnect electrodes. The detailed fabrication process is described in the Supporting Information.

EIS Measurements. The impedance measurements were made by scanning the frequency and recording the impedance and phase on a probe station using tungsten-tipped probes and an impedance meter (HP Agilent 4294A). Typically, the binding interactions were carried out in PBS containing 0.05% tween-20 as a detergent (PBST), and the electrochemical measurements were made in 10 mM PBS containing a redox probe (PBSR) consisting of 2.5 mM each of $K_4[Fe(CN)_6]\cdot 3H_2O$ and $K_3[Fe(CN)_6]$. The oscillation voltage was kept at 25 mV with a dc bias voltage of 220 mV. This optimized combination of the oscillation voltage and dc bias values gave us better results as compared to the usually reported values of 5−10 mV oscillation voltage and 120−230 mV dc bias for faradic EIS biosensors. It is important to optimize these values because it is also a circuit-related issue and is dependent on the concentration of the redox probe coupled in the solution, especially when utilizing a two-electrode system such as interdigitated electrodes.[28,29] A software application was written in Visual Basic to collect EIS data over a frequency range of 50 Hz to 50 kHz at the end of the following events: in PBSR before the sample was incubated, after the incubation of the sample (serum dilution), and after the incubation with colloidal gold labels for signal enhancement. The incubations were carried out in PBST, and the buffer was changed to PBSR before data collection. A series of 80 data points were collected per sweep and averaged for 3 sweeps over a 1 min period. The data was analyzed using Z-View software commercially available from Scribner Associates (Southern Pines, NC, U.S.). The experimental curves were fitted using a suitable Randles electrically equivalent model. All plots were made by exporting the analyzed Z-View data to MS-Excel.

Biofunctionalization. The chips were plasma precleaned and processed as follows. Cysteamine self-assembled monolayers (SAMs) were formed on the gold surface by incubating the chips in a solution of cysteamine hydrochloride (0.01 M in ethyl alcohol) for 8 h. The SAMs were treated with a 1% triethylamine aqueous solution for 30 min, washed with water and PBS, and incubated with 2.5% glutaraldehyde in PBS for 2 h. After the activation of SAM with glutaraldehyde, the chips were washed with carbonate buffer (50 mM, pH 9.6) and incubated with antigen protein (i.e., 50 μg/mL tTG solution) using a silicon channel enclosure around the electrodes. The protein solution was allowed to air dry, and the chips were washed thoroughly with DIW. The unused SAM functional groups were neutralized using 1% ethanolamine in carbonate buffer for 30 min, and the nonspecific binding sites were blocked by using 1% polyvinylpyrrolidone (PVP) in PBST for 1 h. We have used PVP instead of conventional blocking agents such as casein/albumins because of its better performance as reported elsewhere by us and other groups.[27,30] The chips were stored at 4 °C under PBST until used.

Immunosensor Assay. The electrode array was enclosed in a channel consisting of a PDMS well with the contact electrodes extending beyond the well to the contact pads near the edge of the chip. A Plexiglas chamber supporting the inlet/outlet tubes was mechanically held over the PDMS well. The assay was run on the chip, and the data was collected as described in the EIS Measurements section. A typical assay procedure consisted of calculating the initial data in PBSR, injecting goat anti-TG antiserum dilutions made in PBST, incubating for a predetermined time (10 min), washing with PBST and PBSR, and collecting the binding data in PBSR. The data was analyzed as explained above in the EIS Measurements section. The baseline impedance was established by taking average values of impedance before incubation with anti-TG antiserum dilutions. The differential change in impedance due to the specific binding of αTGAbs with respect to baseline impedance was used as the signal for a given dilution of antiserum used. For nanoparticle-based signal enhancement, the Pr-A-GNPs were allowed to bind with captured antibodies for a predetermined time (10 min). The signal enhancement due to the binding of Pr-A-GNPs was determined with respect to baseline impedance and the label-free αTGAbs binding signal.

On-Chip ELISA. An on-chip ELISA procedure was used to compare the sensitivity of a biosensor with that of a conventional enzyme immunoassay. The chips biofunctionalized with tTG were incubated with different concentrations of goat anti-TG antiserum in the flow channel as described in the previous section. After incubation (10 min), the chips were washed with PBST thoroughly and then HRP conjugated rabbit anti-goat-IgG (Sigma, A5420) secondary antibody was injected into the channel at dilutions suggested by the manufacturer. After 20 min of incubation with the secondary antibody, the chips were washed thoroughly with PBST and removed from the flow channel. A subsequent procedure was carried out in a four-quadrant Petri dish. Each chip was transferred to a Petri dish quadrant containing 5 mL of a TMB/H_2O_2 substrate system (Sigma, T0440). The HRP chromogenic substrate reaction (appearance of blue color) was allowed to proceed for 20 min, and then 1 mL of a blue solution was taken out of the Petri dish and the reaction was stopped using 0.5 mL of an acidic stop solution (1N H_2SO_4) that was confirmed by a color change from blue to yellow. The optical density (OD) of the yellow solution was read at a 450 nm wavelength using a spectrophotometer (Shimadzu UV-1800). The color intensity was proportional to the dilution of anti-TG antiserum used.

Colloidal Gold Nanoparticle Labels. Monodisperse (15−20 nm) colloidal gold nanoparticles (GNPs) were prepared by a slight modification of methods published elsewhere.[15,31] Briefly, a 200 mL solution of 0.01% tetrachloroauric acid (gold chloride) in water was brought to boil, and 8 mL of 1% trisodium citrate solution was rapidly added to the boiling gold chloride solution. The solution was allowed to boil for 10 min until it developed the typical bright wine-red color of colloidal gold. As-prepared GNPs ($OD_{525\ nm}$ = 1.49) were conjugated with protein-A (Pr-A) by exploiting charge-based binding with a slight modification of a previously reported method.[32] GNP (40 mL) was adjusted to pH 7.0 using 0.2 M K_2CO_3 and added to 400 μL of a 1 mg/mL protein-A solution in phosphate buffer (pH 7.0). After 15 min, 1 mL of 10% BSA in phosphate buffer (pH 7.0) was added to the solution. The conjugate was concentrated by centrifugation, and the loose pellet of the Pr-A-GNP conjugate was resuspended in phosphate buffer to a final $OD_{525\ nm}$ of 3.0.

III. RESULTS AND DISCUSSION

Device Simulations. The Ansoft Maxwell software was utilized to determine the electromagnetic field distribution on our

Table 1. Geometric Parameters Designed and Materialized for Nanogap IDEs and a Comparison of the Relative Sensitivity of Nanogap IDE Devices to Identical Variations in the Electrochemical Environment

IDE's device ID	W/G of digits designed pattern (nm) (expected P^a)	W/G of digits after pattern development (nm)	final W/G of Au electrode digits (nm) (final P^a)	IDE area in m2 (no. of IDE digits^b)	sensitivity (slope) (aerial sensitivity^c)
D2	400/200 (600)	523.8/188.6	464.1/224.3 (688.4)	8.4×10^{-9} (257)	−30 925 (3.68155×10^{12})
D3	400/400 (800)	484.4/302.7	439.6/355.6 (795.2)	7.0×10^{-9} (225)	−16 651 (2.35957×10^{12})
D4	700/200 (900)	750.6/154.5	696.8/184 (880.8)	9.1×10^{-9} (200)	−14 777 (1.61391×10^{12})
D5	700/300 (1000)	755.5/272.7	708.8/264.3 (973.1)	8.4×10^{-9} (180)	−8925 (1.0625×10^{12})
D6^d	1500/500	1500/500	1500/500	1.78×10^{-8} (80)	−5951 (3.34×10^{11})

^{a} Pitch of IDE = width (W) + gap (G). ^{b} Actual number of digits materialized per IDE. ^{c} aerial sensitivity = slope of curve/area (m^2) ^{d} IDE devices materialized using UVPL only.

devices by using the following equation:

$$\nabla \cdot [\sigma E + j\omega\varepsilon\nabla\phi(x,y)] = 0 = f(x,y) \quad (1)$$

where $f(x, y)$ is the magnitude and phase of the electric potential at each value of x and y, ω is the angular frequency at which the potential is oscillating, σ is the conductivity, and ε is the permittivity. An ac conduction solution was developed using a voltage of 25 mV, a frequency of 60 Hz, and a phase angle of 0°. The boundary is assumed to be insulated from any kind of outside electric/magnetic activity.

Figure 1b shows the change in the strength of the electric field (E, V/m) for an IDE with different W and G combinations of the electrode digits. Device simulation showed that the current density and electric field showed a large change in flux when the gap between the electrodes was decreased to below 800 nm; however, these values remained relatively unaffected by the change in width of the electrode digits. A detailed analysis of different design parameters and simulation results for IDEs has been reported elsewhere.[27] On the basis of the simulated results, IDEs with nanoscale gaps ranging from 100 to 500 nm and widths ranging from 400 to 1500 nm were fabricated.

Sensitivity of Nanogap IDEs. Table 1 shows several different W/G combinations that were designed and fabricated. IDEs with gaps ranging from 150 to 500 nm were materialized and expected to be most sensitive on the basis of the simulation results. Interdigitated digits or "fingers" from opposite electrodes had a length and width of 50 μm and 70 nm, respectively. Each chip was composed of eight sets of IDEs that could be individually connected via contact pads that were designed in a secure digital (SD) card format. These eight IDEs were arranged such that they could also be divided into two groups, where each group could be served by its own flow channel (Figure 1c-i). Individual IDEs were characterized by optical microscopy and a scanning electron microscope (SEM) to ascertain geometric parameters at different stages of fabrication (Figure 1c-ii,c-iii).

The IDEs should be sensitive to the chemical environment around the electrodes in order to be successful as transducers for biosensor applications. The relative sensitivity of IDEs with different geometries was compared by subjecting them to varying concentrations of a redox probe solution. Equimolar solutions of $K_4[Fe(CN)_6]\cdot 3H_2O$ and $K_3[Fe(CN)_6]$ were used with concentrations of 0.01, 0.1, 1.0, 10, and 100 μM. The impedance data was collected, and the Nyquist plots obtained were fitted into the Randles equivalent circuit model as shown in Figure 2a. It was observed that for all devices the charge-transfer resistance (R-Ct) increased with decreasing concentration of the probe solution and maximum R-Ct values were observed for deionized water (DIW). The R-Ct in the presence of a redox probe approached that of DIW at concentrations of ≤1 nM. All devices tested showed a maximum sensitivity in the 0.1 to 10.0 μM range. This range was used to compare the relative sensitivity of the electrodes. As shown in Figure 2b, R-Ct values were plotted against the redox probe concentration and the slope of curve in this range was used as a measure of the sensitivity of the device. Negative values were obtained for the slopes of these curves, indicating an inverse relationship between R-Ct and the probe concentration.

In general, the sensitivity of the IDEs, designated as D2 to D6, decreased with an increase in the pitch P ($P = W + G$) of the IDE devices and agree with the previous reports.[25,27] IDEs with the smallest pitch i.e., D2 was at least 5.25 times more sensitive than D6, the IDEs with largest pitch explored in this study. It is interesting that the sensitivities of IDEs D3 and D4 are relatively close, although with a larger pitch D4 is expected to have a much lower sensitivity but a smaller gap between the digits, appears to be responsible for the enhanced sensitivity of this device. A closer comparison of different device designs revealed that for a given pair of devices with relatively close widths (D2/D3 and D4/D5) the sensitivity was higher for the device with a smaller gap between electrodes. These results agree with expected performance of devices as predicted by the device simulations in our previously reported work[27] concluding the sensitivity will be higher with a smaller gap. To account for the differences in the available area of the different devices, the sensitivity per unit area was calculated and is shown in Figure 2c. The relative aerial sensitivity of the IDE with the smallest pitch (D2) was 11.2 times higher than the sensitivity of D6, which is the IDE with the largest pitch.

Label-Free Biosensor for the Qualitative Detection of *α*tTG-Abs. Celiac disease is an inherited autoimmune disorder that affects the digestive process of the small intestine. When a person who has celiac disease consumes gluten, a protein found in wheat, rye, and barley, the individual's immune system responds by attacking the small intestine and inhibiting the absorption of important nutrients into the body. Undiagnosed and untreated, celiac disease can lead to the development of other autoimmune disorders, as well as osteoporosis, infertility, neurological conditions, and, in rare cases, cancer.[33] The incidence of celiac disease in healthy individuals in the U.S.[34] is 1 in 133; however, among the Asian and Hispanic populations it is 1 in 256. The average length of time it takes for a symptomatic person to be diagnosed with celiac disease in the U.S. is 4 years; this type of delay dramatically increases an individual's risk of developing other autoimmune disorders, neurological problems, osteoporosis, and even cancer. More than 3 million people are affected by

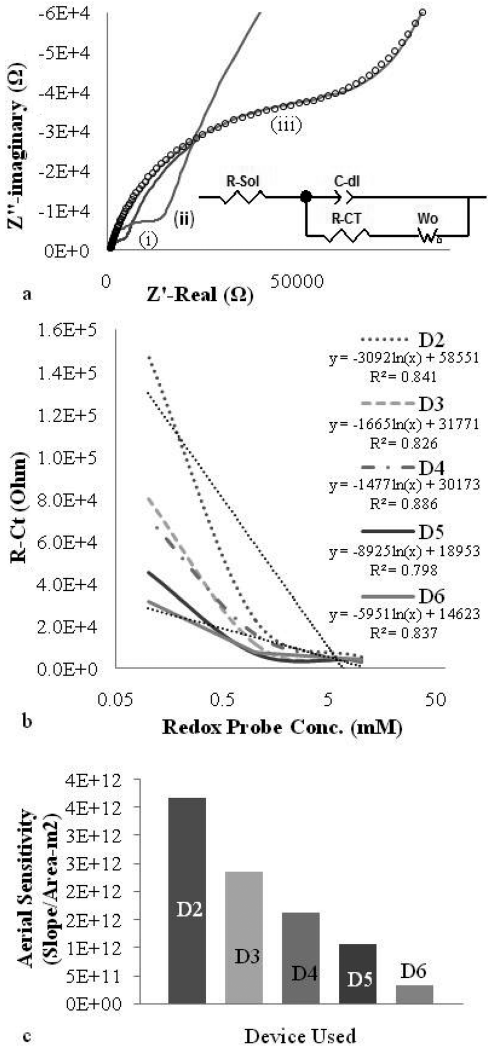

Figure 2. Device sensitivity comparison for devices D2, D3, D4, D5, and D6. (a) Curves i−iii shows Nyquists plots for 0.01, 0.001, and 0.0001 M of the redox probe (shown only for device D6 here). The best fit for each curve (overlapping hollow dots, shown only for curve iii) was used to determine the *R*-Ct values for the Randles equivalent circuit (inset). (b) *R*-Ct values plotted against the redox probe concentrations. For all devices, the slopes of the curves were determined from the best fit equations (shown as a straight lines only for devices D2 and D6 for clarity) for each curve (shown in the legend) and is termed device sensitivity. (c) Relative aerial sensitivites (slope per unit area) of different devices D2−D6 as described in Table 1. Please see the Sensitivity of Nanogap IDEs section for details.

celiac disease and go as long as 11 years before diagnosis.[35] More efforts are required toward developing fast, affordable, and specific screening methods for this disease. αtTG-Abs in serum is an established biomarker of celiac disease.[9] We decided to use αtTG goat serum as a model test sample for the qualitative detection of αtTG-Abs antibodies using nanogap IDEs.

For the detection of αtTG-Abs in serum, antigen tTG was immobilized on the electrode surface as described before for other proteins.[27] αtTG serum dilutions were prepared in buffer (PBST) and allowed to interact with the Ag on the electrodes. The specificity of the detection was confirmed by measuring activity against a nonspecific Ag (OVA). Data was collected before and after the binding of the anti-tTG antiserum dilution. It was observed that *R*-Ct decreased with increasing dilution of the serum sample because the amount of available specific αtTG-Abs also decreased with increasing dilution of the serum sample (Figure 3).

In the case of label-free assays, the *R*-Ct increased with the increase in antibody binding on the electrode surface as evident from the increasing diameter of the semicircular part of the Nyquist plots with the decreasing dilution of serum (Figure 3a). At lower serum dilution, more αtTG-Abs are available to bind at the electrode surface. The average maximum *R*-Ct of 1850 Ω was determined for the least diluted serum sample, and 490 Ω was determined at the maximum dilution with a variation observed at 12−18% (Figure 4c). Although the change in signal was proportional to the change in available αtTG-Abs in the applied sample, the observed binding signal increased only 3.75-fold when the sample concentration changed by 5 orders of magnitude (i.e., from the least dilution of 10^{-2} to the maximum dilution of 10^{-7} part serum in PBST). The on-chip ELISA assay (Figure 3b) showed an 8.8-fold ($OD_{450\ nm}$ changes from 0.307 to 2.7) change in signal over the same range of antiserum dilutions (Figure 3d). This could be attributed to the activity of enzyme labels. However, it is clear that the Ab−Ag interaction alone was not sufficient to design a biosensor sensitive enough to match the sensitivity observed with ELISA.

Colloidal Gold Nanoparticle (GNP) Labels for Biosensor Signal Enhancement. Colloidal gold nanoparticles (GNPs) were employed as labels to enhance the sensor signal in order to match the larger range of signal change observed with on-chip ELISA. Colloidal gold was conjugated to protein-A (Pr-A), a staphylococcal membrane protein that binds very specifically with the Fc region of IgG Abs. This Pr-A-GNPs conjugate can be used as a label for this biosensor because Pr-A binds to the Abs captured on the electrode surface and along with it GNPs also get established on the electrode surface. The concentration of the stock solution of Pr-A-GNPs conjugate was characterized by an $OD_{525\ nm}$ of 4.0, which was used for initial signal enhancement experiments.

The analysis of signal enhancement with Pr-A-GNPs results indicated that the colloidal gold NPs were producing a change in signal that was dependent on the amount of Abs captured on the electrode surface. Interestingly, the observed *R*-Ct decreased after applying Pr-A-GNPs for the low serum dilutions but showed converse behavior at higher serum dilutions where the *R*-Ct increased after the application of Pr-A-GNPs as compared to the their label-free *R*-Ct values. For the lowest serum dilution of 10^{-2}, the average *R*-Ct value as calculated from the best fit of the impedance curve (Figure 4a) was 1520 Ω, which decreased to just about 800 Ω after the application of Pr-A-GNPs. For a higher serum dilution of 10^{-6}, it increased to 850 from 700 Ω after the binding of Pr-A-GNPs. This dual behavior of the GNPs can be explained by considering the fact that at lower serum dilution the higher amount of specific Ab is captured on the electrode surface and so the number of available binding sites for Pr-A-GNPs is quite high and it is possible that some of the nanoparticles get trapped and assimilated into the sensing biomolecular layer itself. The high density of GNPs established on the electrode surface possibly facilitates a low resistance path for electron transfer between the electrodes and the redox-active probe molecules through the network of trapped metallic GNPs and provides an enhanced surface area for the redox reaction, as has been reported previously.[36,37] However, at higher serum dilutions, because of the smaller number of captured Abs, the

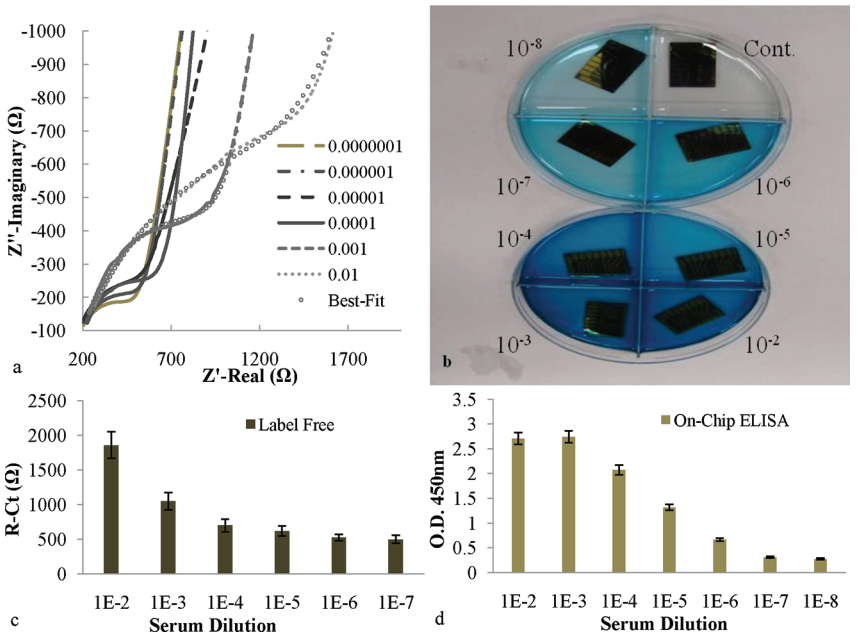

Figure 3. Label-free impedimetric IDEA biosensor assay and on-chip ELISA for the detection of αtTG-Abs in diluted serum. (a) Nyquist plots for different dilutions of serum, with the semicircle diameter increasing with the decreasing dilution of applied sample as the availability of specific Abs increases. (b) On-chip ELISA, with the developed color increasing with the decreasing dilution of serum samples indicating the presence of more Abs bound to the electrodes. (c) *R*-Ct determined by best fitting the Nyquist plots in an equivalent circuit model plotted against the serum dilutions. (d) Optical density at 450 nm recorded and plotted against the serum dilutions. Please see the Label-Free Biosensor for the Qualitative Detection of αtTG-Abs section for details.

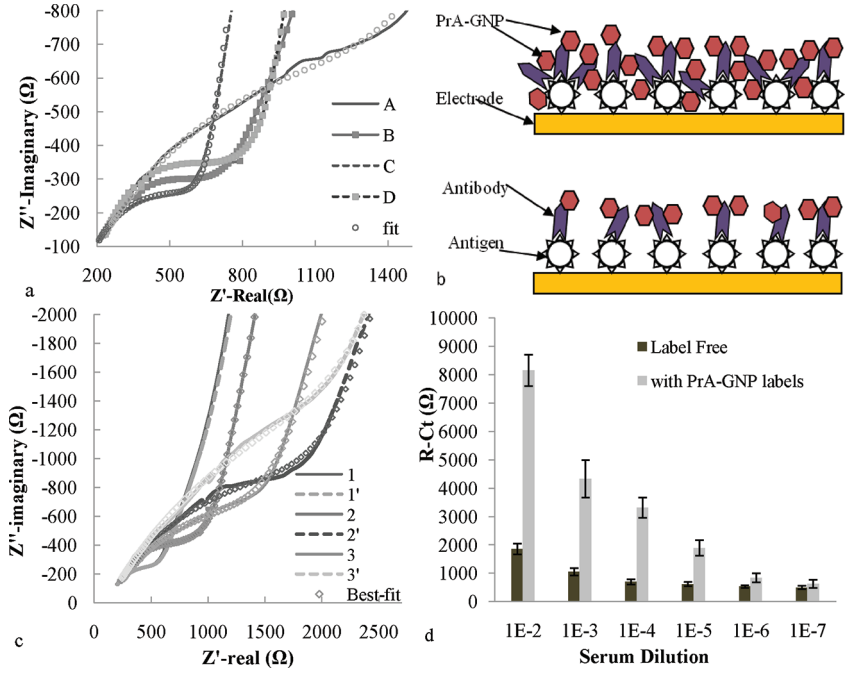

Figure 4. Signal enhancement using Pr-A-GNPs. (a) The use of Pr-A-GNPs at lower serum dilution (10^{-3}) leads to a decrease in the *R*-Ct, curves A and B before and after the binding of Pr-A-GNPs whereas at higher dilution (10^{-6}) the *R*-Ct increases as indicated by the diameter of semicircles in the Nyquist plots, curves C and D. (b) Cartoon depicting the entrapment and assimilation of GNPs in the sensor layers resulting in a low *R*-Ct path at high Ab binding; at low Ab binding, such a possibility is small, leading to an increase in *R*-Ct. (c) Uniform response of enhanced signal (*R*-Ct) over the entire serum dilution range observed when Pr-A-GNP was used at a 1:25 dilution. Curves 1 and 1′, 2 and 2′, and 3 and 3′ are Nyquist plots for 10^{-6}, 10^{-4}, and 10^{-2} part serum in PBST. (d) Signal enhancement of *R*-Ct as determined by fitting the Nyquist plots shown in c using the Randles equivalent circuit (Figure 3a, inset). Please see the Colloidal Gold Nanoparticle Labels for Biosensor Signal Enhancement section for details.

effective density of the GNPs on the electrode surface is much smaller and the networking of metallic NPs that provide a low-resistance path is lost, thereby acting simply as a larger barrier to the flow of electrons thorough multiple protein layers,

dx.doi.org/10.1021/la202546a |*Langmuir* 2011, 27, 13931–13939

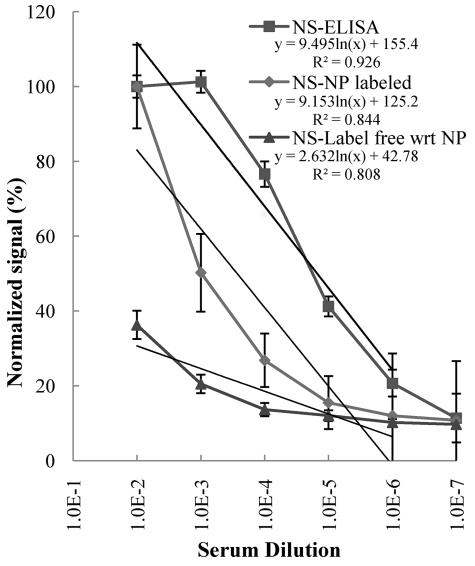

Figure 5. Comparison of bioassay sensitivity using ELISA, label-free, and Pr-A-GNP-labeled biosensors. The readings are normalized with respect to the maximum signal for each assay. The best linear fit was determined, and the equations representing the best fit are shown just below the legends; the slope of the curve from the equations represents the relative sensitivty of the different assays. The error bars represent SD (%) values relative to the actual values observed at the respective serum dilution for that assay. Please see the Comparison of ELISA, Label-Free, and Pr-A-GNP-Labeled Bioassays section for details.

resulting in a net increase in *R*-Ct (Figure 4b). This type of mechanism for the application of GNP-based signal amplification has been previously reported.[38]

Consequently, a dilution of the Pr-A-GNP stock solution of 25-fold was used for all further signal enhancements to reduce the possibility of entrapping GNPs in the signal-generating layer. It was observed that at this dilution of Pr-A-GNP solution the *R*-Ct increased over the whole dilution range of the serum samples (Figure 4c). It was observed that at the lowest serum dilution (10^{-2}) the change in *R*-Ct jumped to an average of 5110 Ω using the Pr-A-GNP label as a secondary reagent whereas at the highest serum dilution (10^{-7}) it increased to only 550 Ω as compared to label-free biosensor assay values of 1850 Ω for the former and 490 Ω for the latter serum dilutions. It was observed that the signal was amplified by 175.6% at the lowest serum dilution and only by 11.2% at the highest serum dilution. Clearly, the signal amplification is proportional to the amount of antibody captured at the electrode surface, which is bound to decrease at higher serum dilutions (Figure 4d).

Comparison of ELISA, Label-Free, and Pr-A-GNP-Labeled Bioassays. In the label-free format, the biosensor signal (i.e., *R*-Ct determined by fitting the experimental results to a Randles equivalent circuit model) changed from 490 Ω at the highest serum dilution (10^{-7}) to 1850 Ω at the lowest serum dilution (10^{-2}). Thus, the signal increased by 3.75-fold over an increase in the sample concentration range spanning 5 orders of magnitude. However, for on-chip ELISA the signal, $OD_{450\ nm}$, increased 8.8-fold over the same concentration range and actually showed signal saturation at one order of concentration less. It was clear that Ab−Ag binding alone was not sufficient to produce a biosensor assay sensitivity comparable to that of ELISA. The use of Pr-A-labeled GNPs increased the sensor signal, when used at appropriate concentration. The use of the Pr-A-GNP label produced an increase in signal of 9.3-fold (from 550 to 5110 Ω) as compared to 3.75- and 8.8-fold for the label-free bioassay and ELISA over the same sample concentration range. Thus, the use of GNP labels brings the biosensor sensitivity closer to that of on-chip ELISA. The sensitivity of the bioassay is generally measured by the slope of the curve. To compare the three different bioassays and their relative sensitivities, the signal values were normalized with respect to the highest value. Figure 5 shows the normalized curves, and a comparison of the slope of the curves shows that the use of GNP labels increases the biosensor assay sensitivity from 2.63 to 9.15 (normalized signal/dil), bringing it quite close to the sensitivity of ELISA at 9.49. ELISA is currently the gold standard for immunoassay and utilizes a label that is catalytic, where a single enzyme molecule can produce plenty of signal-generating events such as the color change from colorless to blue for TMB/H_2O_2 with HRP as the enzyme label. However, the nanopartciles offer a one-time amplification per binding event. The enhanced sensitivity to the level of ELISA is quite significant for fEIS biosensors and a step toward realizing point-of-care electrochemical devices that can eliminate the centralized and sophisticated instrumentation required with ELISA. It should be noted here that the SD values for ELISA were within ±3 to 5% of the average whereas these ranged from ±12 to 18% for the biosensor assay. The impedimetric measurements are prone to inconsistencies, especially because of temperature variations. A detailed temperature-based study has previously been published by our group using impedance spectroscopy and an interdigitated electrode transducer as a biosensor for DNA hybridization.[39] This study compares the DNA hybridization study in the solution phase and on the interdigitated electrode sensor. This study concludes that the IDEs are capable of detecting temperature-induced variations in surface-bound DNA hairpins within the experimental error over a controlled temperature range from 30 to 80 °C. However, our current data represents experiments done in a controlled laboratory environment at room temperature of 72 °F.

The most sensitive region of detection was determined by IC_{50} values (i.e, where the assay signal falls to 50% of the maximum signal): 0.15×10^{-4}, 0.98×10^{-4}, and 2.7×10^{-4} part serum in PBST for ELISA, label-free, and GNP-labeled immunoassays, respectively. These values were determined by solving for x using the equations of best fit as shown in Figure 5 with $Y = 50$. It should be noted that although the labeling improved the sensitivity of the sensor by about 350% in terms of slope by increasing the sensor signal, the lower limit of detection did not change much. The lower limit of detection is apparently determined by the functional affinity of the polyclonal Abs in serum for the immobilized antigen. The reported total Ab concentration in the goat serum is about 20 mg/mL, and the amount of antigen-specific Ab in a polyclonal antiserum is reported from as low as 1% to as high as 24%, with the rest of the pool consisting of normal circulating antibodies.[40] Considering the highest limits, the concentration of tTG-specific Ab in the serum sample can be approximated to a maximum of about 5 mg/mL (i.e., 25% of the total Abs concentration in serum samples). Thus, the sensor platform was roughly tried in the range of a 50 μg/mL (or 300 nM at 10^{-2} dilution of serum) to 50 pg/mL (or 3 pM at 10^{-7} dilution of serum) antibody concentration. Although no quantitative measurements were made, a rough estimation of the dynamic detection range of the sensor would be in the 30 pM to 30 nM antibody concentration. We do not claim here to have

developed a biosensor for celiac sprue, and the choice of the Ag−Ab binding model used here is just coincidental. The efforts to make a multiplexed impedimetric biosensor for the detection of immune -related disorders are being pursued in our laboratory.

IV. CONCLUSIONS

Gold nanoparticles, together with nanogap IDEs, were utilized to demonstrate the enhancement in the biosensor sensitivity. To achieve this, first the effect of geometrical electrode parameters on the sensitivity of IDEs was investigated. It was observed that for IDEs with a constant length having similar widths and heights the gap between the electrodes played a major role in determining the sensitivity of the IDEs to the electrochemical environment. Overall, the aerial sensitivty of IDEs decreased with increasing pitch of the devices. IDEs were used as biosensors using faradaic EIS as a detection technique with αtTG-Abs in serum that are used for the detection of celiac disease as a target analyte. The sensitivity of the IDEs for the label-free detection of the serum biomarker for celiac disease was found to be lacking compared to ELISA, although the sensor and ELISA showed comparable lower limits of detection. Gold nanoparticles were employed as labels to enhance the sensitivity of IDE devices further. It was found that the sensitivity depended on the gold nanoparticle concentration: the smaller concentration of gold nanoparticles increased the sensitivty by 350% over that of the nonlabeled sensor, with an expected dynamic detection range of the sensor in the 30 pM to 30 nM range of Ab in the sample. A comparison with on-chip ELISA showed a comparable lowest detection limit with label-free and GNP-labeled biosensors, whereas the use of GNPs has increased the sensitivity to the level of ELISA. To date, we have not done a detailed study on the effect of nanoparticle size; however, our group is actively pursuing the evaluation of different nanomaterials that can provide more efficient signal amplification as compared to that of metallic GNPs. The primary results for such an evaluation have been reported elsewhere.[41] Nanoscale materials with varied physicochemical properties such as nonmetallic semiconducting (CdS, CdSe, etc.) or dielctric ($SrTiO_3$, SiO_2) and organic (polystyrene, graphene oxide) were compared using standard immunoassay conditions provided by immobilizing normal Abs on the IDEs and Pr-A-NM as the label. The sensitivity may be increased further by using other nanomaterials such as Pr-A-CdS that show a signal amplifictaion that is more than double what is achieved with Pr-A-GNPs under comparable bioaffinity binding studies.

■ ASSOCIATED CONTENT

Supporting Information. Detailed e-beam lithography (EBL) and UV-photolithography (UVPL) procedures and figures showing the fabrication stages of the nanogap-interdigitated electrodes. This material is available free of charge via the Internet at http://pubs.acs.org.

■ AUTHOR INFORMATION

Corresponding Author

*E-mail: kvs.rana@gmail.com.

■ REFERENCES

(1) Self, C. H.; Cook, D. B. Advances in immunoassay technology. *Curr. Opin. Biotechnol.* **1996**, *7*, 60–65.

(2) Wild, D. The Immunoassay Handbook, 3rd ed.; Elsevier: Oxford, U.K., 2005.

(3) Berson, S. A.; Yalow, R. S. Assay of plasma insulin in human subjects by immunological methods. *Nature (London)* **1959**, *184*, 1648–1649.

(4) Engvall, E.; Perlman, P. Enzyme-linked immunosorbent assay (ELISA). Quantitative assay of immunoglobulin G. *Immunochemistry* **1971**, *8*, 871–874.

(5) Van Weemen, B. K.; Schuurs, A. H. Immunoassay using antigen-enzyme conjugates. *FEBS Lett.* **1971**, *15*, 232–236.

(6) Lequin, R. Enzyme immunoassay (EIA)/enzyme-linked immunosorbent assay (ELISA). *Clin. Chem.* **2005**, *51*, 2415–2418.

(7) Bilitewski, U. Protein-sensing assay formats and devices. *Anal. Chim. Acta* **2006**, *568*, 232–247.

(8) Chen, H.; Jiang, C.; Yu, C.; Zhang, S.; Liu, B.; Kong, J. Protein chips and nanomaterials for application in tumor marker immunoassays. *Biosens. Bioelectron.* **2009**, *24*, 3399–3411.

(9) Sblattero, D.; Berti, I.; Trevisiol, C.; Marzari, R.; Tommasini, A.; Bradbury, A.; Fasano, A.; Ventura, A.; Not, T. Human recombinant tissue transglutaminase ELISA: an innovative diagnostic assay for celiac disease. *Am. J. Gastroenterol.* **2000**, *95*, 1253–1257.

(10) Niemeyer, C. M. Nanoparticles, proteins, and nucleic acids: biotechnology meets materials science. *Angew. Chem., Int. Ed.* **2001**, *40*, 4128–4158.

(11) Chan, W. C. W.; Nie, S. Quantum dot bioconjugates for ultrasensitive nonisotopic detection. *Science* **1998**, *281*, 2016–2018.

(12) Turyanska, L.; Bradshaw, T. D.; Sharpe, J.; Li, M.; Mann, S.; Thomas, N. R.; Patanè, A. The biocompatibility of apoferritin-encapsulated PbS quantum dots. *Small* **2009**, *5*, 1738–1741.

(13) Shankar, S. S.; Rai, A.; Ankamwar, B.; Singh, A.; Ahmad, A.; Sastry, M. Biological synthesis of triangular gold Nanoprisms. *Nat. Mater.* **2004**, *3*, 482–488.

(14) You, C. C.; De, M.; Rotello, V. M. Monolayer-protected nanoparticle protein interactions. *Curr. Opin. Chem. Biol.* **2005**, *9*, 639–646.

(15) Kaur, J.; Singh, K. V.; Boro, R.; Thampi, K. R.; Raje, M.; Varshney, G. C.; Suri, C. R. Immunochromatographic dipstick assay format using gold nanoparticles labeled protein-hapten conjugate for the detection of atrazine. *Environ. Sci. Technol.* **2007**, *41*, 5028–5036.

(16) Stoscheck, C. M. Protein assay sensitive at nanogram levels. *Anal. Biochem.* **1987**, *160*, 301–305.

(17) Thanh, N. T. K.; Rosenzweig, Z. Development of an aggregation-based immunoassay for anti-protein A using gold nanoparticles. *Anal. Chem.* **2002**, *74*, 1624–1628.

(18) Tatona, T. A.; Lu, G.; Mirkin, C. A. Two-color labeling of oligonucleotide arrays via size-selective scattering of nanoparticle probes. *J. Am. Chem. Soc.* **2001**, *123*, 5164–5165.

(19) Wang, J.; Xu, D.; Kawde, A. N.; Polsky, R. Metal nanoparticle-based electrochemical stripping potentiometric detection of DNA hybridization. *Anal. Chem.* **2001**, *73*, 5576–5581.

(20) Sadik, O. A.; Aluoch, A. O.; Zhou, A. Status of biomolecular recognition using electrochemical techniques. *Biosens. Bioelectron.* **2009**, *24*, 2749–2765.

(21) Kojima, K.; Hiratsuka, A.; Suzuki, H.; Yano, K.; Ikebukuro, K.; Karube, I. Electrochemical protein chip with arrayed immunosensors with antibodies immobilized in a plasma-polymerized film. *Anal. Chem.* **2003**, *75*, 1116–1122.

(22) Chen, X.; Wang, Y.; Zhou, J.; Yan, W.; Li, X.; Zhu, J. J. Electrochemical impedance immunosensor based on three-dimensionally ordered macroporous gold film. *Anal. Chem.* **2008**, *80*, 2133–2140.

(23) Bothara, M.; Venkatraman, V.; Reddy, R.; Barrett, T. W.; Carruthers, J.; Prasad, S. Nanomonitors: electrochemical immunoassays for protein biomarker profiling. *Nanomedicine* **2008**, *3*, 423–436.

(24) Montelius, L.; Tegenfeldt, J. O.; Ling, T. G. Fabrication and characterization of a nanosensor for admittance spectroscopy of biomolecules. *J. Vac. Sci. Technol., A* **1995**, *13*, 1755–1760.

(25) Gerwen, P. V.; Laureyn, W.; Laureys, W.; Huyberechts, G.; Beeck, M.; Baert, K.; Suls, J.; Sansen, W.; Jacobs, P.; Hermans, L.; Mertens, R. Nanoscaled interdigitated electrode arrays for biochemical sensors. *Sens. Actuators, B* **1998**, *49*, 73–80.

(26) Kim, S. K.; Hesketh, P. J.; Li, C.; Thomas, J. H.; Halsall, H. B.; Heineman, W. R. Fabrication of comb interdigitated electrodes array (IDA) for a microbead-based electrochemical assay system. *Biosens. Bioelectron.* **2004**, *20*, 887–894.
(27) Singh, K. V.; Whited, A. M.; Ragineneni, Y.; Barrett, T.; King, J.; Solanki, R. 3D interdigitated electrode array biosensors. *Anal. Bioanal. Chem.* **2010**, *397*, 1493–1502.
(28) Pei, R.; Cheng, Z.; Wang, E.; Yang, X. Amplification of antigen−antibody interactions based on biotin labeled protein−streptavidin network complex using impedance spectroscopy. *Biosens. Bioelectron.* **2001**, *16*, 3 55–361.
(29) Barton, A. C.; Davis, F.; Higson, S. P. J. Labeless immunosensor assay for the stroke marker protein neuron specific enolase based upon an alternating current impedance protocol. *Anal. Chem.* **2008**, *80*, 9411–9416.
(30) Haycock, J. W. Polyvinylpyrrolidone as a blocking agent in immunochemical studies. *Anal. Biochem.* **1993**, *208*, 397–399.
(31) Frens, G. Controlled nucleation for the regulation of the particle size in monodispersed gold suspensions. *Nat. Phys. Sci.* **1973**, *241*, 20–22.
(32) Horisberger, M.; Clerc, M. F. Labeling of colloidal gold with protein A. *Histochem. Cell Biol.* **1985**, *82*, 219–223.
(33) Green, P. H. R.; Stavropoulos, S. N.; Panagi, S. G.; Goldstein, S. L.; Mcmahon, D. J.; Absan, H.; Neugut, A. I. Characteristics of adult celiac disease in the USA: results of a national survey. *Am. J. Gastroenterol.* **2001**, *96*, 126–131.
(34) Fasano, A.; Berti, I.; Gerarduzzi, T.; Not, T.; Colletti, R. B.; Drago, S.; Elitsur, Y.; Green, P. H.; Guandalini, S.; Hill, I. D.; Pietzak, M.; Ventura, A.; Thorpe, M.; Kryszak, D.; Fornaroli, F.; Wasserman, S. S.; Murray, J. A.; Horvath, K. Prevalence of celiac disease in at-risk and not-at-risk groups in the United States: a large multicenter study. *Arch. Intern. Med.* **2003**, *163*, 286–292.
(35) Rampertab, S. D.; Pooran, N.; Brar, P.; Singh, P.; Green, P. H. Trends in the presentation of celiac disease. *Am. J. Med.* **2006**, *119*, 355. e9–14.
(36) Wang, M. J.; Wang, L. Y.; Wang, G.; Ji, X. H.; Bai, Y. B.; Li, T. J.; Gong, S. Y.; Li, J. H. Application of impedance spectroscopy for monitoring colloid Au-enhanced antibody immobilization and antibody−antigen reactions. *Biosens. Bioelectron.* **2004**, *19*, 575–582.
(37) Guo, S.; Dong, S. Biomolecule-nanoparticle hybrids for electrochemical biosensors. *Trends Anal. Chem.* **2009**, *28*, 96–109.
(38) Chen, H.; Jiang, J. H.; Huang, Y.; Deng, T.; Li, J. S.; Shen, G. L.; Yu, R. Q. An electrochemical impedance immunosensor with signal amplification based on Au-colloid labeled antibody complex. *Sens. Actuators, B* **2006**, *117*, 211–218.
(39) Micusan, V. V.; Borduas, A. G. Biological properties of goat immunoglobulins G. *Immunology* **1977**, *32*, 373–381.
(40) Horisberger, M.; Clerc, M. F. Labeling of colloidal gold with protein A. *Histochem. Cell Biol.* **1985**, *82*, 219–223.
(41) Singh, K. V.; Dash, S.; Whited, A.; Solanki, R. Evaluation of Nanomaterials-Biomolecule Hybrids for Signal Enhancement of Impedimetric Biosensors. *IEEE Nano-2011*, Aug 15−18, 2011, Portland, OR. (www.ieeenano2011.org)